Effects of initial-state laser excitation on inner-shell photoionization and Auger decay of Rb

K. Jänkälä,[1,*] J. Schulz,[1,2] M. Huttula,[1] A. Caló,[1] S. Urpelainen,[1] S. Heinäsmäki,[1] S. Fritzsche,[3] S. Svensson,[2] S. Aksela,[1] and H. Aksela[1]

[1]*Department of Physical Sciences, P.O. Box 3000, 90014 University of Oulu, Oulu, Finland*

[2]*Department of Physics, Uppsala University, Box 530, SE-75121 Uppsala, Sweden*

[3]*Department of Physics, University of Kassel, Heinrich-Plett-Strasse 40, D-34132 Kassel, Germany*

(Received 7 July 2006; published 7 December 2006)

The $3d^{-1}$ photoionization and subsequent $M_{4,5}N_{2,3}N_{2,3}$ Auger electron spectra of free initially laser-excited rubidium atoms have been investigated. The rubidium atoms were excited from the ground state $[Kr]5s_{1/2}$ to the $[Kr]5p_{1/2}$ and $[Kr]5p_{3/2}$ states. Emphasis was put on the changes in coupling and electron correlation between the three different initial states. The ground state $3d$ photoelecton spectrum of free Rb atoms was interpreted in detail. The binding energies for $3d_{3/2,5/2}$ orbitals of initially ground-state and laser-excited Rb atoms were obtained. Extensive multiconfiguration Dirac-Fock calculations performed in the relativistic *jj* coupled basis were compared to the experimental photoelectron and Auger electron spectra.

DOI: 10.1103/PhysRevA.74.062704 PACS number(s): 32.80.Hd, 32.80.Fb, 31.25.Eb, 31.25.Jf

I. INTRODUCTION

Selective initial state laser excitation combined with high brilliance synchrotron radiation ionization has proven to be an efficient way to study structures and dynamics of free atoms. Studies with initially laser-prepared alkali-metal atoms have been of interest during the last couple of years. They have included the valence shell ionization of Na [1,2], K [3], Rb [4], and Cs [5]. In Ref. [6] emphasis was put on the inner-shell photoionization and Auger decay of K. Simultaneous study of photoelectron spectra (PES) and Auger electron spectra (AES) in Refs. [6,7] was found to be an effective way to probe changes to inner-shell processes due to laser excitation.

In alkali-metal atoms the first two excitations $ns_{1/2} \rightarrow np_{1/2,3/2}$ increase the orbital angular momentum of the outermost electron by one. This changes the coupling of the electron total angular momentum to the holes created by ionization and Auger processes. The electron in the excited orbital is also less bound to the atom, which changes the correlation and exchange effects between the electrons. In this work we have studied these effects experimentally and theoretically in the $3d$ photoionization and subsequent $M_{4,5}N_{2,3}N_{2,3}$ Auger decay of initially excited and nonexcited Rb.

To the best of our knowledge, no experimental $3d$ photoelectron spectrum has been reported for atomic Rb. Previously $3d_{3/2,5/2}$ binding energies of atomic Rb have been determined using calculations and photoabsorption by Connerade and Mansfield [8] and later based on the same experimental data by Mårtensson and Johansson [9]. The $M_{4,5}N_{2,3}N_{2,3}$ Auger spectrum of ground state Rb has been studied previously experimentally and theoretically by Aksela *et al.* [10]. Due to large correlation, even the main structures of the $M_{4,5}N_{2,3}N_{2,3}$ Auger spectrum of Rb were found to be exceptionally difficult to calculate. Similar difficulties have also been reported in the calculation of the $3d$ absorption spectra of Rb [11].

*Electronic address: kari.jankala@oulu.fi

II. EXPERIMENT

The PES and AES measurements of atomic Rb were performed at the high resolution undulator beamline I411 [12], at the MAX-II 1.5 GeV synchrotron storage ring in Lund, Sweden. The exciting photon source was a tunable vanadate laser pumped Ti:Sa laser medium which allowed a tuning range of 1.2–1.8 eV. The range was sufficient to excite Rb atoms from the ground state $[Kr]5s_{1/2}$ to the $[Kr]5p_{1/2}$ state at the photon energy of 1.560 eV and to the $[Kr]5p_{3/2}$ state at the energy of 1.589 eV.

The emitted electrons were measured using the experimental setup built in Oulu [13], which has been upgraded by replacing the electron spectrometer with a Scienta SES-100 hemispherical analyzer. The beam of Rb atoms was prepared by a resistively heated oven at 110–115 °C and the ejected photo and Auger electrons were measured at the magic angle of 54.7° with respect to the polarization vector of the linearly polarized synchrotron radiation.

In the case of $3d$ PES measurements, the ionizing synchrotron beam was monochomatized to the photon energy of 200 eV with a modified Zeiss SX-700 plane grating monochomator [14,15]. A recent update of the beamline monochomator control allowed us to use the plane grating only as a mirror. The widths of the Auger spectrum lines are not sensitive to the ionization source bandwidth. Therefore using the first-order undulator peak without monochromatization we were able to obtain exceedingly high count rate to the $M_{4,5}N_{2,3}N_{2,3}$ AES of Rb. Within the same counting time, roughly twenty times higher intensity was obtained to the AES by using the plain undulator peak. In these measurements the first harmonic undulator peak was set to the photon energy of 165 eV, in order to avoid overlapping of the photoelectron lines caused by the higher-order undulator harmonics.

The $3d$ PES were measured with a constant pass energy of 20 eV, the beamline slit was set to 30 μm, and the entrance slit of the spectrometer was 0.8 mm (curved). In these settings the spectrometer broadening was estimated to be about 100 meV. In the case of AES measurements, the high

intensity allowed us to use a pass energy of 10 eV. The spectrometer entrance slit used was the same as in the PES measurements. The spectrometer broadening of AES lines was estimated to be about 38 meV. Since the natural linewidth of $M_{4,5}N_{2,3}N_{2,3}$ AES lines of Rb are over 80 meV [10], we can state that by simply improving the spectrometer resolution one cannot obtain more details in the ground-state Auger spectra.

The binding energy calibration for the PES was obtained from the Kr $3d_{3/2,5/2}$ photoelectron lines [16] and the kinetic energy calibration for the AES by using Kr $M_{4,5}N_{2,3}N_{2,3}$ AES [17]. The transmission correction curve for AES was obtained experimentally [18] by using the $3d_{3/2,5/2}$ photoelectron and the $N_{4,5}O_{2,3}O_{2,3}$ Auger electron lines of Xe.

III. THEORY AND CALCULATIONS

The calculations were performed by using the multiconfiguration Dirac-Fock (MCDF) method, where the atomic state functions (ASFs) are generated as linear combinations from the relativistic *jj* coupled configuration state functions (CSFs)

$$\Psi_\gamma(PJM) = \sum_i c_{\gamma i}\psi_i(PJM). \tag{1}$$

In Eq. (1), the labels (PJM) state that the linear combination is formed from the CSFs with the same parity and total angular momentum. Numerical calculations were done by applying the GRASP92 code [19] together with the RELCI extension [20]. The GRASP92 code optimizes the wave functions of the many-electron Dirac-Coulomb Hamiltonian and diagonalizes the Dirac-Coulomb-Breit Hamiltonian in a second step to account further relativistic corrections. The initial radial wave functions were obtained from the Thomas-Fermi model and the calculations were performed in the average level (AL) scheme.

The relative photonization cross sections were obtained by using an approximate expression for the Bethe-Born cross section (see, e.g., Ref. [21]),

$$Q_\beta(J_\beta) = (2J_\beta + 1)\left|\sum_{\nu\alpha} c_{\beta\nu}c_{i\alpha}\delta_{X_\nu X_\alpha}\right|^2. \tag{2}$$

In Eq. (2) $c_{i\alpha}$ and $c_{\beta\nu}$ denote the mixing coefficients of the initial and final ASFs, respectively. X_ν refers to the final-state configuration and X_α to the same parent configuration in the initial state. For more details, see the Appendix of Ref. [22]. Based on the sudden approximation, the intensities of the monopole shakeup transitions were obtained by weighting the relative cross sections obtained on the direct photoemission from Eq. (2) with a squared overlap integral between the initial- and final-state orbitals of the outermost electron. The intensities of the conjugate shakeup transitions were not calculated.

According to the two-step model, the relative intensity of the emitted Auger electrons to the magic angle can be expressed as

$$n_{f\beta}(J_f,J_\beta) = \frac{T_{f\beta}(J_f,J_\beta)Q_\beta(J_\beta)}{P_\beta(J_\beta)}, \tag{3}$$

where $Q_\beta(J_\beta)$ is the relative photoionization cross section, $P_\beta(J_\beta)$ is the total decay rate of the initial state and

$$T_{f\beta}(J_f,J_\beta) = 2\pi\sum_{l_A j_A}\left|\sum_{\mu\nu} c_{f\mu}c_{\beta u}M_{f\beta}^{\mu\nu}\right|^2 \tag{4}$$

is the Auger decay rate. The transition amplitude $M_{f\beta}^{\mu\nu}$ is the Coulomb matrix element where the operator inside is the Coulomb operator, initial state is the singly ionized state, and final state is the doubly ionized atomic state which is coupled to the continuum electron to yield the same parity as the initial state. For more details, see Ref. [21]. Numerical calculations of Eq. (3) were done by using the AUGER component of the RATIP package [23].

The calculations were performed by generating ASF sets in AL scheme to each ionization state. In the calculation of the neutral-state wave function, the configurations $[\mathrm{Kr}](4d^1,5s^1,5p^1,5d^1,6s^1,6p^1,6d^1,7s^1)$ were included. In order to reduce shifting of the average energy the calculations were performed in two steps. In the first step, the wave functions of the Rb atom were computed in a single configuration approximation and in the second step the radial wave functions of the [Kr]-like core were fixed and the outer orbitals were generated. The $3d^{-1}$ ionized state was computed in a similar way by including the configurations $[\mathrm{Kr}(3d^{-1})]\{4d^1,5s^1,5p^1,5d^1,6s^1,6p^1,6d^1,7s^1\}$. In the second step, the last orbital fixed was $3p$. In the doubly ionized state, the configurations used were $[\mathrm{Kr}(4d^{-2})]\{4d^1,5s^1,5p^1,5d^1,6s^1,6p^1,6d^1,7s^1\}$, $[\mathrm{Kr}(4p^{-3})]\{5s^2,5s^15p^1\}$, $[\mathrm{Kr}(4s^{-1}4p^{-2})]\{5s^2,5s^15p^1\}$, and $[\mathrm{Kr}(4s^{-1})]$. In this case the initial-core wave functions were obtained from the single configuration calculation, but in the second step, all orbitals were set to free in a multiconfiguration iteration.

IV. RESULTS AND DISCUSSION

A. 3*d* photoelectron spectrum of Rb

The experimental ground-state $3d$ PES of Rb is shown in Fig. 1. The vertical bars denote the intensities obtained from the least square fit using Voigt functions. Energies and relative intensities of the peaks are given in Table I. Energies of the structures 9 and 10 are averages of the energies of the two lines used to fit the peaks. The identifications of the lines were done by comparing the experimental spectrum to the MCDF calculations. Also, information from the spectra of initially excited atoms was used to confirm some of the assignments.

In the following we use the notation $nl_j^{-k}ml^r_{j,[J_1,\ldots,J_n]}$, where j denote the orbital angular momenta and J_i the total ionic states angular momenta. The main peaks 12 and 13 come from the direct photoionization of the $3d_{3/2}$ and $3d_{5/2}$ orbitals, respectively. The splitting of peaks 12 and 13 into the fine-structure lines $3d_{3/2}^{-1}5s_{1/2,[1,2]}$ and $3d_{5/2}^{-1}5s_{1/2,[2,3]}$ is too small to be observed experimentally. The small structure 11 on the left-hand side of peak 12 arises from mixing of the

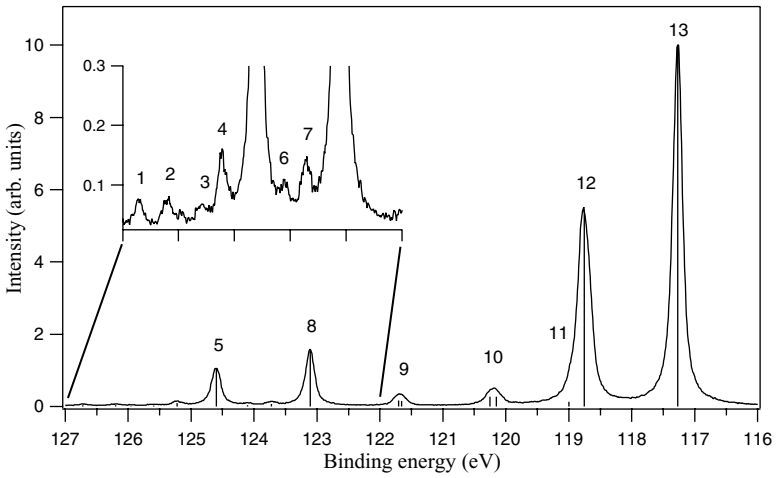

FIG. 1. Experimental $3d$ photoelectron spectrum of Rb measured at the photon energy of 200 eV. For better visualization the binding energy region of 122–127 eV is magnified.

lines $3d_{3/2}^{-1}5s_{1/2,[1,2]}$ to the lines $3d_{5/2}^{-1}4d_{3/2,[2]}$ and $3d_{5/2}^{-1}4d_{5/2,[1]}$ in the final state of photoionization. The obtained $3d_{3/2}$ and $3d_{5/2}$ binding energies 118.76(5) and 117.25(5), respectively, agree well with the previously determined values of 118.76(10) and 117.33(5) [8] and of 118.70(5) and 117.26(5) [9].

At the binding energies over 120 eV, the satellite structure is mainly caused by shakeup transition of the $5s_{1/2}$ electron during photoionization. The structures corresponding to shakeup transitions appear in pairs divided by the same $3d_{3/2}^{-1}$ and $3d_{5/2}^{-1}$ spin-orbital splitting as the main lines. The two highest satellite peaks 5 and 8 are due to the $5s_{1/2} \rightarrow 3d^{-1}6s_{1/2}$ monopole shakeup transitions. Peaks 9 and 10 come from the conjugate $5s_{1/2} \rightarrow 3d^{-1}5p_{1/2,3/2}$ shakeup transitions. Two lines were needed to fit the separate peaks 9 and 10 because of the splitting of the $5p$ orbital in the final state. Peak 1 and partially peak 4 rise from the $5s_{1/2} \rightarrow 3d^{-1}7s_{1/2}$ monopole shakeup transition. The other part of peak 4 and of peak 7 come from the $5s_{1/2} \rightarrow 3d^{-1}5d_{3/2,5/2}$ conjugated shakeup transitions and peaks 3 and 6 rise from the $5s_{1/2} \rightarrow 3d^{-1}6p_{1/2,3/2}$ transitions. Peak 2 remained unidentified, but is most likely due to the $5s_{1/2} \rightarrow 3d_{5/2}^{-1}8s_{1/2}$ transition.

TABLE I. Experimental energies and relative intensities of the $3d^{-1}$ photoelectron lines of Rb. Assignments denote the final configurations of the photoionization.

Label	Assignment	Energy (eV)	Intensity
1	$3d_{3/2}^{-1}7s_{1/2}$	126.7(1)	0.42
2	⋯	126.2(1)	0.42
3	$3d_{3/2}^{-1}6p_{1/2,3/2}$	125.6(1)	0.27
4	$3d_{5/2}^{-1}7s_{1/2}+3d_{3/2}^{-1}5d_{3/2,5/2}$	125.2(1)	1.01
5	$3d_{3/2}^{-1}6s_{1/2}$	124.60(5)	10.39
6	$3d_{5/2}^{-1}6p_{1/2,3/2}$	124.1(1)	0.45
7	$3d_{5/2}^{-1}5d_{3/2,5/2}$	123.7(1)	0.78
8	$3d_{5/2}^{-1}6s_{1/2}$	123.11(5)	15.29
9	$3d_{3/2}^{-1}5p_{1/2,3/2}$	121.7(1)	3.22
10	$3d_{5/2}^{-1}5p_{1/2,3/2}$	120.2(1)	5.51
12(11)	$3d_{3/2}^{-1}5s_{1/2}(3d_{5/2}^{-1}4d_{3/2,5/2})$	118.76(5)	55.58
13	$3d_{5/2}^{-1}5s_{1/2}$	117.27(5)	100

B. PES of $5s_{1/2} \rightarrow 5p_{1/2,3/2}$ excited Rb

Figure 2 shows three intensity normalized $3d^{-1}$ PES, measured with laser off, laser in the $5s_{1/2} \rightarrow 5p_{1/2}$ resonance, and in the $5s_{1/2} \rightarrow 5p_{3/2}$ resonance. The normalization peak 13 (see Fig. 1) was chosen so that it does not contain overlapping intensity from the laser excited atoms. The laser does not reach all the atoms in the interaction region. Instead, the constant atomic density is redistributed to the excited and nonexcited parts. Thus the spectrum measured with laser on is a mixture of these two parts and scaling is needed to be able to substract out the nonexcited part. Because of the large overlap of the structures 10 and L3 and structure 12 and peak L4 in Fig. 2, observation of the initially excited spectra is easier if the nonexcited part of the spectrum is subtracted out. These subtracted spectra are shown in Figs. 3(a) and 3(b). The normalization procedure used leads to an overestimation of the signal coming from the excited atoms, if the true count rates are used. In this study, overestimation is not a problem because only the relative intensities are considered.

The largest changes in the spectra due to the laser excitation are denoted by labels L1–L4 in Fig. 2. The labels refer to both laser-on spectra. The structures labeled as L1 and L2 denote the satellite structures caused mainly by the $5p_{1/2,3/2} \rightarrow 3d^{-1}6p_{1/2,3/2}$ transitions and labels L3 and L4 denote the main lines of the spectra from initially excited atoms. The peaks L3 and L4 appear at higher binding energy than the main lines 12 and 13 (see Fig. 1) from the nonexcited atoms. The energy differences of the excited and nonexcited states is due to the different screening caused by the electrons to the nuclear potential and the laser photon energy. The energy difference between lines L3 and L4 and the conjugated shakeup lines 9 and 10 in Fig. 1 from ground-state atoms is the same as the initial state excitation energy because the lines have the same final states. This confirms that the lines 9 and 10 are caused by $5s_{1/2} \rightarrow 3d^{-1}5p_{1/2,3/2}$ transitions. The same study to the known satellite lines L1 and L2 confirms that the lines 3 and 6 are indeed caused by $5s_{1/2} \rightarrow 3d^{-1}6p_{1/2,3/2}$ transitions.

Due to small statistical mismatches between the nonexcited part of the spectra in Fig. 2, the difference spectra in Figs. 3(a) and 3(b) show some anomalous behavior (negative

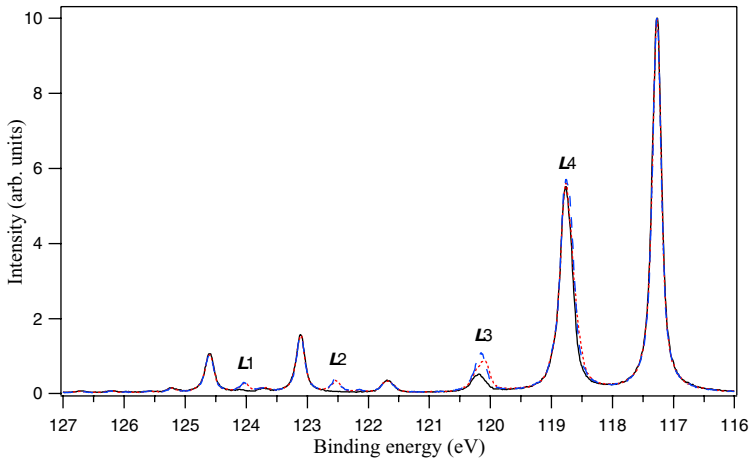

FIG. 2. (Color online) Experimental $3d$ PES of Rb measured with laser on and off. The solid line is the ground-state spectrum, the dotted red line is the spectrum measured with laser in $5s_{1/2} \rightarrow 5p_{1/2}$ resonance, and the dashed blue line is the spectrum measured with laser in $5s_{1/2} \rightarrow 5p_{3/2}$ resonance at laser polarization angle of 45° with respect to the synchrotron polarization.

intensities) when the intensity contribution from nonexcited atoms changes rapidly and the experimental error is at the highest in Fig. 2. From the deviation of the dots in Figs. 2(a) and 2(b) one can estimate the statistical errors of the subtracted spectra, which is roughly at least twice the error of the original spectra. The solid lines are obtained from the fits done for the laser on spectra by keeping the nonexcited contribution fixed in the fits. In addition to the assignments in Fig. 2, small peaks L5 and L6 can be seen in the difference spectra in the binding energies of 123.6 eV and 122.2 eV. The peaks can be identified to be caused by $5p_{1/2} \rightarrow 3d^{-1}5d_{3/2,5/2}$ and $5p_{3/2} \rightarrow 3d^{-1}5d_{3/2,5/2}$ conjugate shakeup transitions.

By comparing the excited spectra in Fig. 3 and Table II and the ground-state spectrum in Fig. 2 and Table I one can see that the probability for the outermost electron to shakeup via $nl \rightarrow (n+1)l$ monopole transition is clearly enhanced in the excited cases. This behavior can be explained by the sudden approximation model. The calculated overlapping of the $5s_{1/2}$ single electron orbital with the $6s_{1/2}$ orbital in the initial and final states, respectively, in the nonexcited case is much smaller than the overlapping of the $5p_{1/2}-6p_{1/2}$ and $5p_{3/2}-6p_{3/2}$ orbitals in the initially excited cases. The same behavior of the shakeup probabilities was also found in the previous studies of Na [24] and Li [25]. On the other hand, it can be seen from Tables I and II that the probability for electron to shakeup via conjugated shakeup transition from the $5s_{1/2}$ orbital to the $5p_{1/2,3/2}$ orbitals in ground-state case is almost the same as the probability for conjugated shakeup transition from the $5p_{1/2,3/2}$ orbitals to the $5d_{3/2,5/2}$ orbitals in

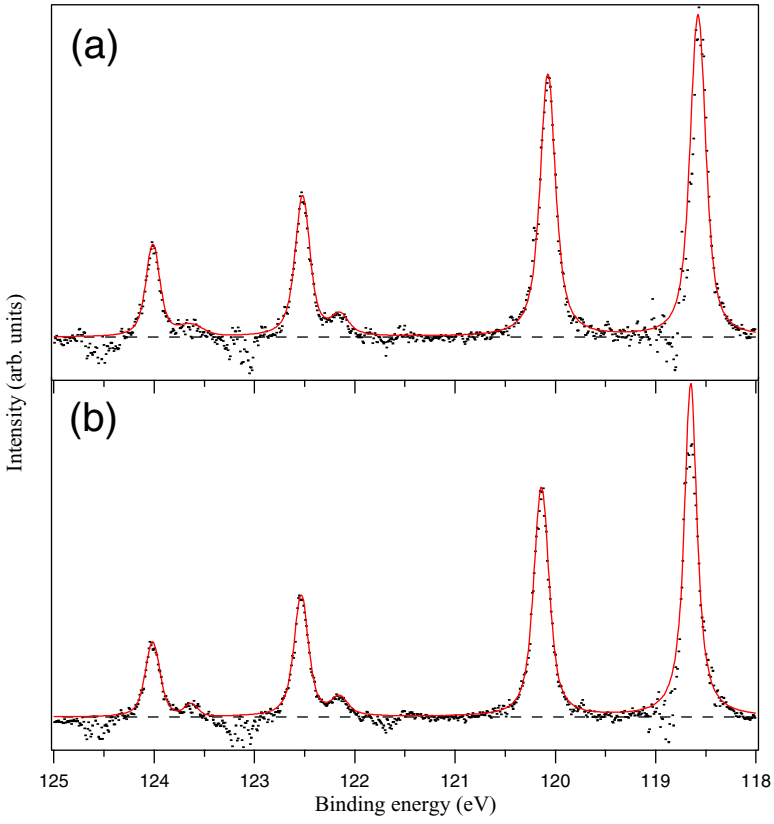

FIG. 3. (Color online) Subtracted spectra between (a) laser in $5s_{1/2} \rightarrow 5p_{1/2}$ resonance and laser off spectrum, (b) laser in $5s_{1/2} \rightarrow 5p_{3/2}$ resonance and laser off spectrum. Dots are the original data points, solid lines are the fits, and the dashed lines denote the zero level.

TABLE II. Experimental and calculated binding energies and relative intensities of the $5p_{1/2}$ and $5p_{3/2}$ excited $3d^{-1}$ photoelectron spectra of Rb.

	Expt. binding energy (eV)		Calc. binding energy (eV)		Expt. relative intensity		Calc. relative intensity	
Label	$Rb^*(5p_{1/2})$	$Rb^*(5p_{3/2})$	$Rb^*(5p_{1/2})$	$Rb^*(5p_{3/2})$	$Rb^*(5p_{1/2})$	$Rb^*(5p_{3/2})$	$Rb^*(5p_{1/2})$	$Rb^*(5p_{3/2})$
*L*1	124.01	124.01	125.25	125.25	25.8	22.9	18.4	18.4
*L*2	122.52	122.53	123.70	123.72	42.0	38.1	27.6	27.9
*L*3	120.08	120.14	121.53	121.57	83.0	76.2	66.1	66.8
*L*4	118.58	118.65	119.97	120.05	100	100	100	100
*L*5	123.63	123.63			4.3	2.4		
*L*6	122.15	122.15			7.0	6.6		

the excited case. A commonly used model for the conjugated shakeup transition is a simultaneous dipole transition and electron excitation to the continuum (see, e.g., Ref. [26]). This indeed implies that the probability should not change much between the nonexcited and excited cases, because the shakeup probability is now proportional to the overlap of the inner-shell electron and continuum and the dipole matrix element of the outermost electron. These quantities are not expected to be very sensitive to the state of the outermost electron.

Figure 4(a) shows the fit lines from Fig. 3 in the same figure and Fig. 4(b) shows the calculated spectra. The calculated spectra are shifted by 1.41 eV to coincide with the experiment. The constant energy shift used for both calculated spectra is due to the AL scheme used. The intensities were calculated using Eq. (2), and the relative intensities between two excited states were not computed. The calculated initially $5p_{1/2}$ excited spectrum is therefore scaled down to better represent the experiment. The small intensity difference between the two measured excited spectra comes from the differences of the excitation cross sections, tuning of the laser to the different wavelengths, alignment of the laser polarization in $5p_{3/2}$ excited case, and various other experimental parameters. The relative differences between the two spectra in energy arise from both the initial- and final-state energy differences. If the initial-state energy difference is taken into account, the energy differences of the main lines L3 and L4 between the two excitations corresponding the same core hole state is about the same as the energy differences between the two lines used to fit the separate peaks 9 and 10 in Fig. 1. This indicates that in the initially nonexcited case, the probability for the electron in $5s_{1/2}$ orbital to shakeup either to the $5p_{1/2}$ or to the $5p_{3/2}$ orbital via conjugated transition is almost the same. Thus, the selective

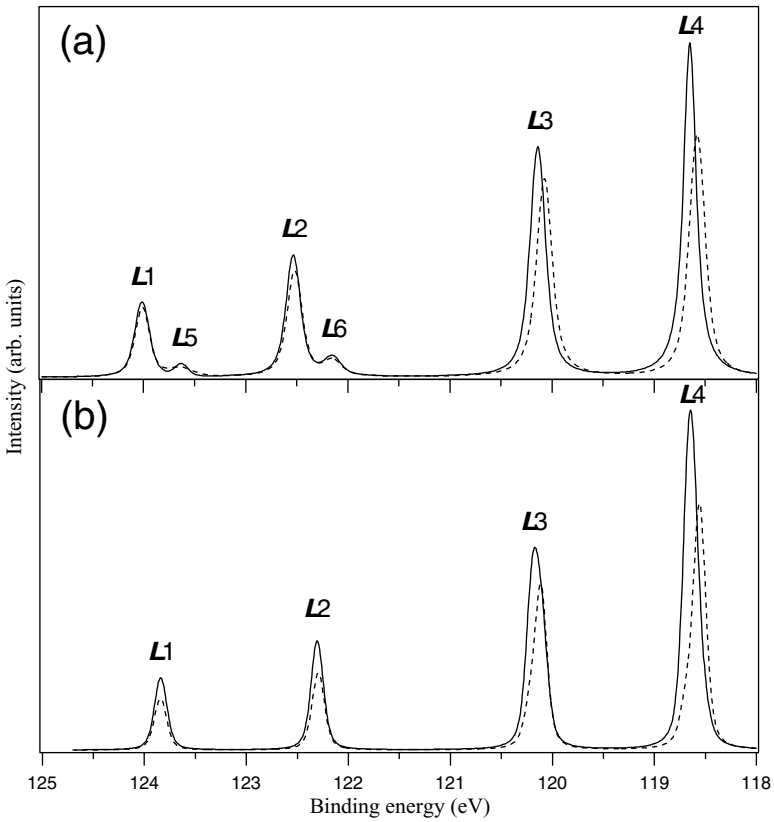

FIG. 4. Fit to the experimental spectra (a) and (b) calculated $3d^{-1}$ PES from initially $5p_{1/2}$ excited (dashed lines) and $5p_{3/2}$ excited (solid lines) Rb. The labels refer to the peaks at the same energy range in the two spectra from $5p_{1/2}$ and $5p_{3/2}$ initial states in (a) and (b).

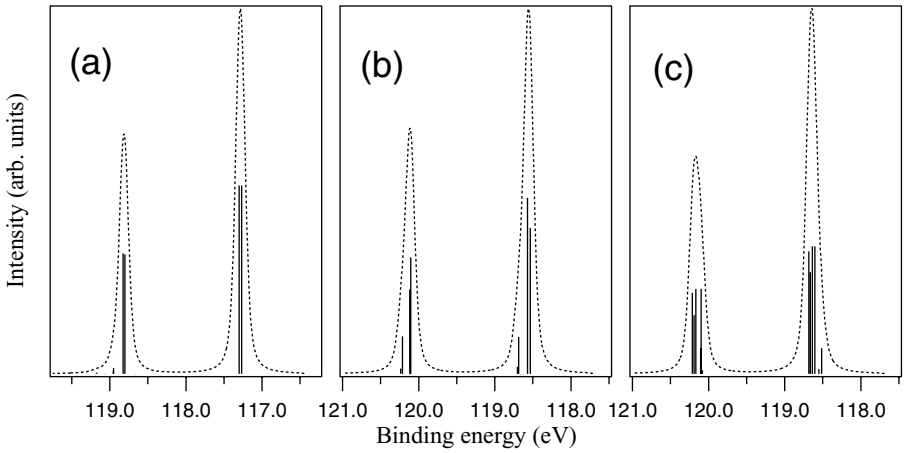

FIG. 5. Calculated $3d^{-1}_{3/2,5/2}$ photoemission main lines from the (a) $K(5s_{1/2})$ initial state, (b) $K^*(5p_{1/2})$ excited initial state, and (c) $K^*(5p_{3/2})$ excited initial state of Rb.

initial-state laser excitation allows one to observe experimentally some highly overlapping lines in the ground-state case.

In general, the calculated spectra in Fig. 4(b) agree well with the experiment in Fig. 4(a). The relative energy differences between the $5p_{1/2}$ and $5p_{3/2}$ excited initial states agree very well, even though the energy differences are of the magnitude of 0.1 eV, as is seen from Table II. The calculated relative energies of the monopole shakeup lines disagree by about 0.2 eV from the experimental values. Correct prediction of the energies of the satellite lines in the inner-shell ionization was found to be difficult also in the previous studies (see, e.g., Ref. [6]). Even the large MCDF calculations in the AL scheme seem to underestimate the energy differences between the main and satellite lines.

The individual fine-structure lines cannot be directly observed experimentally, due to the large natural linewidth of the core-ionized states, and one has to rely on the calculations. The calculated $3d^{-1}_{3/2,5/2}$ main peaks from the three different initial states are plotted in Figs. 5(a)–5(c). The dashed lines show similar behavior when compared to each other, but the calculated individual lines creating the profiles are very different in each case. In Fig. 5(a) the peaks are mainly formed by two lines due to the coupling of the $5s_{1/2}$ electron to a $3d$ hole, giving $3d^{-1}_{3/2}5s_{1/2,[1,2]}$ and $3d^{-1}_{5/2}5s_{1/2,[2,3]}$ states. In the $5p_{1/2}$ excited case, shown in Fig. 5(b), the single configuration jj coupling gives four lines with the same total J values as in the nonexcited case. The lines are also divided into two groups $3d^{-1}_{3/2}5p_{1/2,[1,2]}$ and $3d^{-1}_{5/2}5p_{1/2,[2,3]}$. The mixing between $3d^{-1}_{3/2}5p_{1/2,[1,2]}$ and $3d^{-1}_{3/2}5p_{3/2,[1,2]}$ states gives intensity to two and $3d^{-1}_{5/2}5p_{1/2,[2,3]}$ and $3d^{-1}_{5/2}5p_{3/2,[2,3]}$ mixing to other two smaller lines seen on the left-hand side of the main lines. Similar behavior of the $2p$ photoemission lines was also obtained in the $4s_{1/2}\rightarrow 4p_{1/2}$ initially excited potassium [6]. Figure 5(c) shows the calculated main lines from the $5p_{3/2}$ excited Rb. This case is slightly more complicated, because the jj coupling gives rise to eight lines divided into two groups $3d^{-1}_{3/2}5p_{3/2,[0,1,2,3]}$ and $3d^{-1}_{5/2}5p_{3/2,[1,2,3,4]}$. The same configuration mixing as in the $5p_{1/2}$ excited case also applies to the $5p_{3/2}$ excited case. The calculations indicate that the outermost electron most likely conserves its total angular momentum in the $3d$ photoionization, but in the case of $5p_{1/2}$ excitation there is about 15% probability for an electron to change to the higher $j=3/2$ state and in the case of $5p_{3/2}$ excited electron about 7% probability to change to the lower $j=1/2$ state. The lower probability for spin flip in the $5p_{3/2}$ excited case can be understood from the higher number of possible final states. The mixed final states with the total $J=1,2$ obtain in total half the intensity of those in the $5p_{1/2}$ excited case and therefore the spin flip probability is also lower.

In the recent studies of final-state selection in $3p$, $4p$, and $5p$ photoemission of laser excited K [3], Rb [4], and Cs [5], clear differences between final states with the same core hole j but different total J were found. According to calculations of the inner-shell photoionization of Rb, similar final-state selection does not seem to occur. The initial state J_0 angular momentum influences the final-state structure, but the final states with different J and the same core hole angular momentum j divide the intensity almost equally.

C. AES of $5s_{1/2}\rightarrow 5p_{1/2,3/2}$ excited Rb

Three $M_{4,5}N_{2,3}N_{2,3}$ AES of Rb measured with laser off, laser in $5s_{1/2}\rightarrow 5p_{1/2}$ resonance and in $5s_{1/2}\rightarrow 5p_{3/2}$ resonance are shown in Fig. 6. The spectra measured with laser on are normalized in the same way as the PES in the previous section. Due to the overlapping of the excited and ground-state contributions, comparison between the spectra is again easier if the ground-state part is subtracted from the spectra measured with laser on. Figure 7(a) shows the pure initially excited contributions from both laser on spectra seen in Fig. 6. Figure 7(b) displays the calculated AES from initially $5p_{1/2}$ and $5p_{3/2}$ excited states. For visualization, the $5p_{1/2}$ excited spectrum in Fig. 7(b) is scaled down.

The sticks in Fig. 6 display the fitted lines of the ground state $M_{4,5}N_{2,3}N_{2,3}$ AES of Rb. Single-configuration coupling gives 8 CSFs to the $4p^{-2}5s$ final states. It is clear that the single-configuration approximation cannot reproduce all the structures seen in the experimental spectrum. Some of the complexity arises from overlapping and mixing of the final state $4s^{-1}5s^0$ and satellite structures [10].

The AES with laser in $5s_{1/2}\rightarrow 5p_{3/2}$ resonance was taken with laser polarization angles of 45° and 135° with respect to synchrotron polarization. No significant effects due to laser polarization were found and all the spectra were summed. Due to this, it can be noted from Fig. 7(a) that the statistical noise is considerably lower in the spectrum with laser in

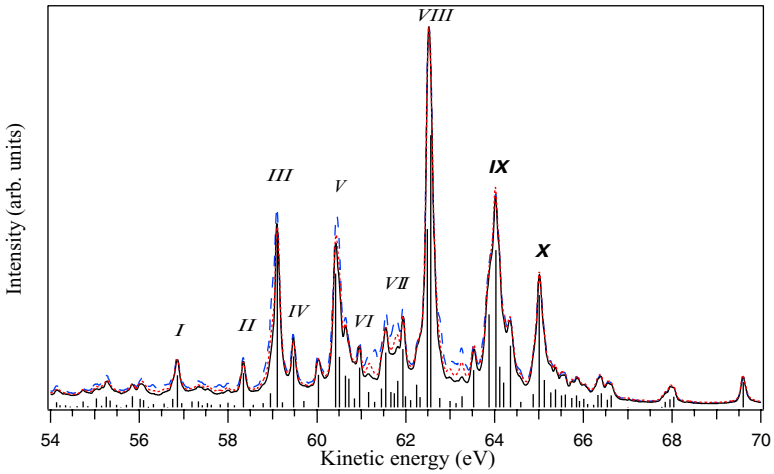

FIG. 6. (Color online) Experimental $M_{4,5}N_{2,3}N_{2,3}$ Auger spectra of Rb measured with laser on and off. The solid black line is the ground-state spectrum, the dotted red line is the spectrum measured with laser in $5s_{1/2}\rightarrow 5p_{1/2}$ resonance, and the dashed blue line is the spectrum measured with laser in $5s_{1/2}\rightarrow 5p_{3/2}$ resonance. The sticks denote the lines obtained from the fit done to the ground-state spectrum.

$5s_{1/2}\rightarrow 5p_{3/2}$ resonance than in $5s_{1/2}\rightarrow 5p_{1/2}$ resonance.

By comparing the ground-state spectrum in Fig. 6 and the two initially excited spectra in Fig. 7(a), it can be seen that at first glance the difference between the three spectra is significant. Closer study using theoretical results reveals that the main structures divided by the coupling of $4p^{-2}$ holes in the ground-state spectrum also appear in the excited spectra, but some of the structures are modified due to changes in the coupling of the outermost electron and mixing of configurations. The structures IV and VI in Fig. 6 correspond to peaks LI and LII in Fig. 7(a), peaks VIII and IX in Fig. 6 are divided into groups of three peaks LIII and LIV in Fig. 7(a) and the peak X correspond to structures LV. The corresponding structures to I–III, V, and VII are missing entirely from the excited spectra in Fig. 7(a).

The calculated spectra in Fig. 7(b) agree well with the experimental spectra in Fig. 7(a) and especially the structures LIII and LIV are predicted remarkably well. Computed AES lines from three different initial states are compared to each other in Figs. 8(a)–8(c). The areas of the spectra are scaled to be equal. For visualization, the spectra of excited Rb in Figs. 8(b) and 8(c) are shifted 1.2 eV towards higher energies to coincide with the corresponding structures in the spectrum in the uppermost panel. In Fig. 8(a) the peaks i and ii correspond to peaks I and II in the experimental spectrum in Fig. 7(a). The peaks I and II rise from transitions to the same final states from the initial states $3d_{5/2}^{-1}5s_{1/2,[2,3]}$ and $3d_{3/2}^{-1}5s_{1/2,[1,2]}$, respectively. The leading term of the final state ASF is $4p^{-2}4d_{3/2,[1/2]}^{1}$ with the purity of only 0.25. The $4d$ configuration can interact with $5s$ but not with $5p$, therefore the peaks I and II do not appear in the spectra in Figs. 7.

The peaks iii and iv in Fig. 8(a) appear as peaks i_1^* and ii_1^* in Fig. 8(b) and as i_2^* and ii_2^* in Fig. 8(c). In all three cases the largest contributions to the peaks comes from transitions to a

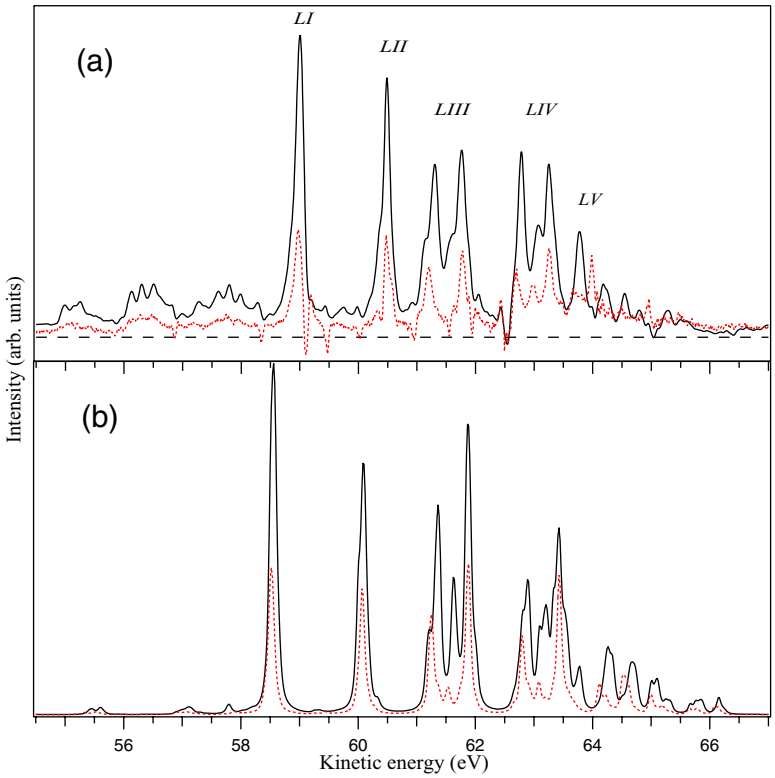

FIG. 7. (Color online) Experimental (a) and (b) calculated $M_{4,5}N_{2,3}N_{2,3}$ AES from initially $5p_{1/2}$ excited (dotted red lines) and $5p_{3/2}$ excited (solid black lines) Rb. The dashed line in (a) denotes the zero level.

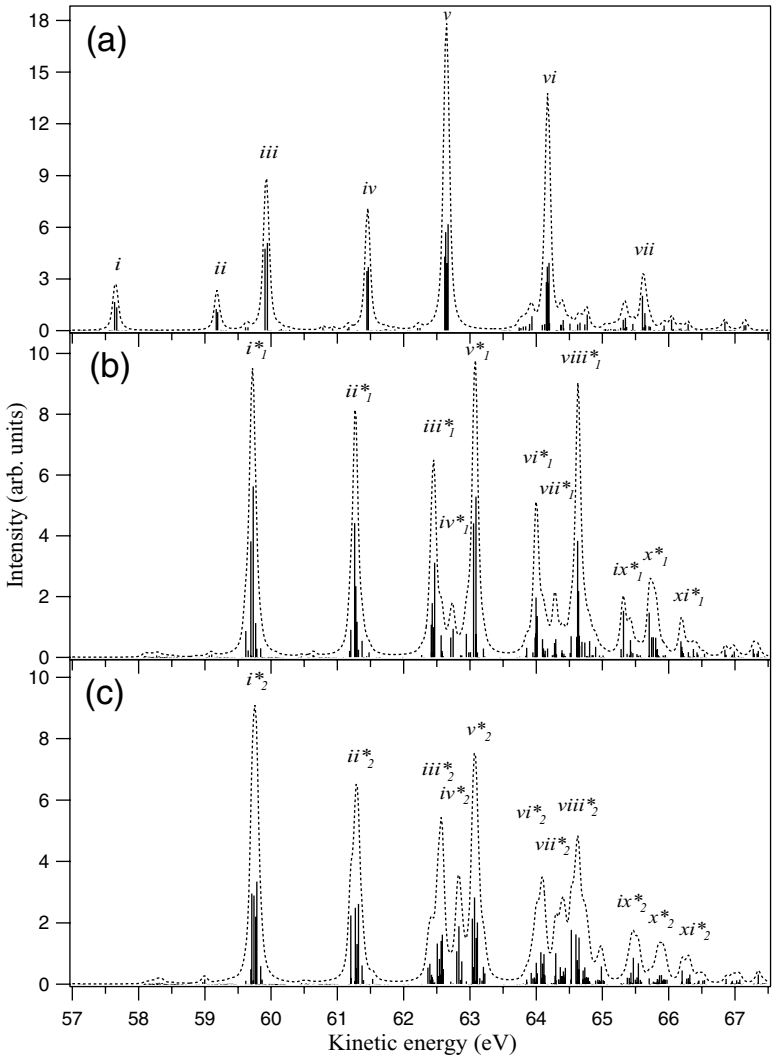

FIG. 8. Calculated $M_{4,5}N_{2,3}N_{2,3}$ AES from (a) nonexcited states, (b) initially $5p_{1/2}$ excited states, and (c) $5p_{3/2}$ excited states of Rb. The spectra in panels (b) and (c) are shifted 1.2 eV.

single final state and therefore splitting and internal structure is defined by the initial states. In the nonexcited atom the final state is $4p^{-2}5s_{1/2,[1/2]}$, in initially $5p_{1/2}$ excited Rb $4p^{-2}5p_{1/2,[1/2]}$ and in $5p_{3/2}$ excited Rb $4p^{-2}5p_{3/2,[3/2]}$.

Reference [10] suggested that peaks III and V in Fig. 6 correspond to the calculated peaks iii and iv, respectively. This is not correct, because observed splitting of the peaks III and V is 1.33 eV and from the photoelectron spectrum in Fig. 1 it is known that the splitting of transitions leading to the same final state is 1.49 eV. Identification of lines iii and iv as corresponding to IV and VI, respectively, fulfills this condition. It agrees also with the optically observed final-state values from Ref. [27]. From Fig. 6 can be seen that small contribution to peaks III and V comes from the Auger decays of $3d^{-1}5p_{1/2,3/2}$ states. From calculations it can be obtained that partial intensity to peaks III and IV may rise from $3d^{-1}6s_{1/2} \rightarrow 4p^{-2}6s_{1/2}$ transitions.

Calculation of ground-state $M_{4,5}N_{2,3}N_{2,3}$ Auger spectrum of Rb was found to be a difficult task in the previous study [10]. Comparing experiment from Fig. 6 and theory from Fig. 8(a), it can be seen also that in this study the agreement is not very good. One possible reason is mixing between $4p^{-2}-4s^{-2}$ and $4p^{-2}-4p^{-4}4d^2$ final states. Including the $4s^{-2}5s_{1/2}$ and $4p^{-4}4d^25s_{1/2}$ states in the calculations caused some effects to the Auger spectra, but the total agreement was not improved. Difficulties in the calculations arise also from the calculation of the $5s$ orbital, because Auger calculations using the same wave functions reproduces experimentally observed $5p_{1/2}$ and $5p_{3/2}$ excited Auger spectra remarkably well, which can be seen from Figs. 7(a) and 7(b). One considerable reason for better agreement is the different parity of the p and d orbitals which reduces the electron correlation in the excited cases. Another reason is the larger radial expectation value of the outermost electron in the excited cases.

The structure LIII in Fig. 7(a) corresponds to peak VIII in the ground-state spectrum in Fig. 6. Similar splitting of some of the AES lines in the excited case was also obtained in potassium [6], but no explanation was suggested. According to calculations, peak v consists of a pair of two lines in Fig. 8(a). The peak is a sum of transitions from the initial states $3d_{5/2}^{-1}5s_{1/2,[2,3]}$ to the final states $4p^{-2}(j=2)5s_{1/2,[3/2]}$ and $4p^{-2}(j=2)5s_{1/2,[5/2]}$. The j in brackets denote the coupled angular momenta of the two holes is the $4p$ shell, which is coupled to produce the total angular momenta J of the final ionic state. Since the spatial angular momentum of the electron in $5s_{1/2}$ orbital is 0, the energy difference of the final states arises from the coupling of the spin momentum to the

two holes in the $4p_{1/2,3/2}$ orbitals. The energy difference of the two final states obtained from the calculations is only 36 meV. In the $5p_{1/2}$ excited case the contribution to peak iii_1^* in Fig. 8(b) comes from transitions from the initial states $3d_{5/2}^{-1}5p_{1/2,[2,3]}$ to the final state $4p^{-2}(j=2)5p_{1/2,[3/2]}$. Peak v_1^* arises from transitions from the same initial states to the $4p^{-2}(j=2)5p_{1/2,[5/2]}$ final state. The *jj* coupling gives identical j and total J quantum numbers to the nonexcited and $5p_{1/2}$ excited cases, but the experiment gives the splitting of the final states $4p^{-2}(j=2)5p_{1/2,[3/2,5/2]}$ of 0.63 eV. The energy splitting of peaks vi_1^* and viii_1^* is the same as peaks iii_1^* and v_1^*, since the peaks rise from transitions to the same final states, but from the $3d_{3/2}5p_{1/2,[1,2]}$ initial states. The increase of the energy splitting of the final states originates from the change in the coupling of the outermost electron, even though the intermediate j and final J values are the same in the two cases. Peak iv_1^* in Fig. 8(b) does not have its counterpart in the ground-state spectrum. It is not clearly visible in the structure LIII in Fig. 7(a), but the peak in the middle of structure LIV comes from transitions to the same final states. Peaks iv_1^* and vii_1^* rise from mixing of the configurations $4p^{-2}(j=2)5p_{3/2,[3/2]}$ and $4p^{-2}(j=2)5p_{1/2,[3/2]}$ in the final state. Mixing of the configurations allows an electron to spin flip during Auger emission, since the initial states of peaks iv_1^* and vii_1^* are $3d_{5/2}^{-1}5p_{1/2,[2,3]}$ and $3d_{3/2}^{-1}5p_{1/2,[1,2]}$, respectively.

In the $5p_{3/2}$ excited case in Fig. 8(c) the peaks i_2^* and ii_2^* arise from transitions to the same final state and are therefore not divided. The energy splitting of the peaks iii_2^* and v_2^* is in $5p_{3/2}$ excited spectrum 0.51 eV. The highest intensity final state of the structure iii_2^* is $4p^{-2}(j=2)5p_{3/2,[5/2]}$, and of the peak v_2^* $4p^{-2}(j=2)5p_{3/2,[7/2]}$. The angular momentum value $l=1$ of the outermost electron causes again splitting of the lines, but in this case the parallel coupling of the outermost electron angular and spin momenta to $j=3/2$ and to the total angular momentum of $J=5/2$ or $J=7/2$ reduces the splitting when compared to $5p_{1/2}$ excited case. One reason for this behavior is in the radial wave functions. The radial expectation value of the $5p_{1/2}$ orbital is slightly smaller than that of the $5p_{3/2}$ orbital, which indicates stronger correlation with the two holes in the $4p_{1/2,3/2}$ orbitals. Peak iv_2^* is caused by transitions to the same final state as peak iv_1^*. In the initially $5p_{3/2}$ excited case the transition does not require spin flip of the outermost electron and the relative intensity of the peak is considerably higher. The change in the intensity is also well seen in the structure LIII in Fig. 7(a). In the $5p_{3/2}$ excited final states, the same mixing which caused the peak iv_1^* in $5p_{1/2}$ excited case, causes structures on the left-hand side of peak iii_2^* and on the right-hand side of peak v_2^*. This distributed intensity can also be seen in structure LIII in the $5p_{3/2}$ excited experimental spectrum in Fig. 7(a). Peaks vi_2^*, vii_2^*, and viii_2^* can be treated similarly, because the only difference is again in the initial states.

As shown above, in alkali-metal atoms, studying the divided lines of the excited AES and comparing them to the ground-state AES, information of the internal structures of the lines in ground-state AES can be obtained, in principle, without calculations. The lines which are not divided in the excited case are formed by transitions to the single final state and the split lines are caused by transitions to at least two different final states. If the angular momentum of the valence shell electron in ground-state case is nonzero or the shell holds more than one electron, the situation is more complicated and needs to be studied further.

V. CONCLUSIONS

The $3d$ photoelectron spectra of ground state, $5s_{1/2} \rightarrow 5p_{1/2}$ and $5s_{1/2} \rightarrow 5p_{3/2}$ excited Rb atoms were measured. With the aid of MCDF calculations and the spectra from excited atoms, the structures of the $3d$ photoelectron spectrum of ground-state Rb were interpret in high precision. Internal structures of the main $3d$ photoemission peaks from three different initial states were studied theoretically and MCDF calculations were found to predict the energy changes caused by excitation very well. Using MCDF calculations the main structures of $M_{4,5}N_{2,3}N_{2,3}$ Auger spectra of excited Rb atoms were identified. Higher l quantum number of the outermost electron was found to cause splitting of some of the close lying lines, even when the total angular momenta of the electron does not differ from the ground-state case. Theoretical predictions of the Auger spectra of laser excited Rb atoms were found to be in better agreement to the experiment than for ground-state Rb atoms. Considerable mixing between $5p_{1/2}$ and $5p_{3/2}$ excited states was found to be well accounted by calculations, but the correlation and mixing for nonexcited Rb atoms were found to be very difficult to take properly into account.

ACKNOWLEDGMENTS

This work has been financially supported by the Research Council for Natural Sciences of the Academy of Finland, the Swedish Research Council (VR), the Swedish Foundation for Strategic Research (SSF), and NordForsk. K.J. would like to thank Tauno Tönning and Magnus Ehrnroot foundations. The staff of MAX-lab is acknowledged for assistance during the measurements.

[1] D. Cubaynes, M. Meyer, A. N. Grum-Grzhimailo, J.-M. Bizau, E. T. Kennedy, J. Bozek, M. Martins, S. Canton, B. Rude, N. Berrah, and F. J. Wuilleumier, Phys. Rev. Lett. **92**, 233002 (2004).

[2] J. Schulz, M. Tchaplyguine, T. Rander, O. Björneholm, S. Svensson, R. Sankari, S. Heinäsmäki, H. Aksela, S. Aksela, and E. Kukk, Phys. Rev. A **72**, 010702(R) (2005).

[3] M. Meyer, D. Cubaynes, F. J. Wuilleumier, E. Heinecke, T. Richter, P. Zimmermann, S. I. Strakhova, and A. N. Grum-Grzhimailo, J. Phys. B **39**, L153 (2006).

[4] J. Schulz, M. Tchaplyguine, T. Rander, H. Bergersen, A. Lindblad, G. Öhrwall, S. Svensson, S. Heinäsmäki, R. Sankari, S.

Osmekhin, S. Aksela, and H. Aksela, Phys. Rev. A **72**, 032718 (2005).
[5] J. Schulz, M. Määttä, S. Heinäsmäki, M. Huttula, R. Sankari, E. Kukk, T. Rander, S. Svensson, S. Aksela, and H. Aksela, Phys. Rev. A **73**, 062721 (2006).
[6] K. Jänkälä, R. Sankari, J. Schulz, M. Huttula, A. Caló, S. Heinäsmäki, S. Fritzsche, T. Rander, S. Svensson, S. Aksela, and H. Aksela, Phys. Rev. A **73**, 022720 (2006).
[7] M. Richter, J. M. Bizau, D. Cubaynes, T. Menzel, F. J. Wuilleumier, and B. Carré, Europhys. Lett. **12**, 35 (1990).
[8] J. P. Connerade and M. W. D. Mansfield, Proc. R. Soc. London, Ser. A **348**, 539 (1976).
[9] N. Mårtensson and B. Johansson, J. Phys. B **14**, L37 (1981).
[10] H. Aksela, S. Aksela, R. Lakanen, J. Tulkki, and T. Åberg, Phys. Rev. A **42**, 5193 (1990).
[11] M. W. D. Mansfield and J. P. Connerade, J. Phys. B **15**, 503 (1982).
[12] M. Bässler, A. Ausmess, M. Jurvansuu, R. Feifel, J.-O. Forsell, P. de Tarso Fronseca, A. Kivimäki, S. Sundin, and S. L. Sorensen, Nucl. Instrum. Methods Phys. Res. A **469**, 382 (2001).
[13] M. Huttula, M. Harkoma, E. Nõmmiste, and S. Aksela, Nucl. Instrum. Methods Phys. Res. A **467-468**, 1514 (2001).
[14] R. Nyholm, S. Svensson, J. Nordgren, and A. Flodström, Nucl. Instrum. Methods Phys. Res. A **246**, 267 (1986).
[15] S. Aksela, A. Kivimäki, R. Nyholm, and S. Svensson, Rev. Sci. Instrum. **63**, 1252 (1992).
[16] G. C. King, M. Tronc, F. H. Read, and R. C. Bradford, J. Phys. B **10**, 2479 (1977).
[17] L. O. Werme, T. Bergmark, and K. Siegbahn, Phys. Scr. **6**, 141 (1972).
[18] J. Jauhiainen, A. Ausmees, A. Kivimäki, S. J. Osborne, A. Naves de Brito, S. Aksela, S. Svensson, and H. Aksela, J. Electron Spectrosc. Relat. Phenom. **69**, 181 (1994).
[19] F. A. Parpia, C. Froese Fischer, and I. P. Grant, Comput. Phys. Commun. **94**, 249 (1996).
[20] S. Fritzsche, C. Froese Fischer, and G. Gaigalas, Comput. Phys. Commun. **148**, 103 (2002).
[21] A. Mäntykenttä, H. Aksela, S. Aksela, J. Tulkki, and T. Åberg, Phys. Rev. A **47**, 4865 (1993).
[22] M. Huttula, E. Kukk, S. Heinäsmäki, M. Jurvansuu, S. Fritzsche, H. Aksela, and S. Aksela, Phys. Rev. A **69**, 012702 (2004).
[23] J. Nikkinen, S. Fritzsche, and S. Heinäsmäki, Comput. Phys. Commun. **175**, 348 (2006).
[24] D. Cubaynes, J. M. Bizau, F. J. Wuilleumier, B. Carré, and F. Gounand, Phys. Rev. Lett. **63**, 2460 (1989).
[25] Z. Felfli and S. T. Manson, Phys. Rev. Lett. **68**, 1687 (1992).
[26] G. Snell, M. Martins, E. Kukk, W. T. Cheng, and N. Berrah, Phys. Rev. A **63**, 062715 (2001).
[27] C. E. Moore, *Atomic Energy Levels*, Natl. Bur. Stand. Circ. No 467 (U.S. GPO, Washington D.C., 1949), Vol. 1.